UNITED STATES DEPARTMENT OF THE INTERIOR

GEOLOGICAL SURVEY

Geochemical enrichment vectors applied to manganese oxide phases in the northern Pacific

by

Joseph Moses Botbol*

Open-File Report 87 - 197

*Branch of Atlantic Marine Geology
Quissett Campus
Woods Hole, MA 02543
(617) 548-8700

1987

CONTENTS

LIST OF FIGURES (all in pocket)

LIST OF TABLES

1. ABSTRACT

A method of treating geochemical enrichments as vectors has been developed and is based on the premises that, for any given sample, the geochemical enrichment of a variable can be treated as a vector and that the enrichments of two or more variables in a sample compose a vector set whose resultant is the net enrichment vector (NEV) of the sample. For each sample the object is to compute a single number representing the NEV of multiple variables such that the number is the sum of weighted enrichments of the selected variables, and the weights are coefficients derived from correlations between all pairs of those variables in a model.

Co, Ni, and Mn analyses for approximately 1,200 northern Pacific Ocean Mn-rich samples [nodules and (or) crusts] from the Scripps Institution of Oceanography's Sediment Data Bank were used as subject data. Spatial distributions of NEV's for the single elements Co, Ni, and Mn and for the element combinations Co-Mn, Co-Ni, Ni-Mn, and Co-Ni-Mn were computed and plotted.

In part, the unielemental NEV distributions agree with present literature regarding distribution of concentrations of these elements in the northern Pacific. Distributions of all NEV's containing Co are dominated by the broad range of Co enrichment. High positive Ni shows marked affinity for the deeper parts of the study area, and Mn shows no visible significant enrichment at the selected contour levels.

Future efforts will be focused on establishment of transformations that facilitate multivariate enrichment vector interpretations, on development of rejection/inclusion discriminants for variables, and on the use of image processing techniques for data filtering and portrayal.

2. INTRODUCTION

The analytical procedure presented here was designed to facilitate and enhance interpretation of multivariate geochemical data. The procedure involves conversion of selected concentrations to enrichments and, for each sample, expresses the aggregate of these enrichments as a single number.

Co, Ni, and Mn concentrations in manganese-rich samples from the northern Pacific ocean were used as subject data. Both the procedure and the test data have undergone perfunctory testing and scrutiny. Rigorous testing by thorough and varied applications has not yet been completed, therefore this report is considered a preliminary one.

All algorithmic expressions presented in this report are written in "C" programming language notation. All computer programs used for the procedures in this report are programmed in the "C" programming language, and are operational on a computer driven by the UNIX operating system.

3. ACKNOWLEDGEMENTS

This writer is indebted to Dr. Richard B. McCammon (USGS) for his contribution to the development of the analytical method. Dr. Robert G. Garrett (Canadian Geological Survey) provided helpful suggestions regarding application of geochemical enrichment vectors as compared with other multivariate methods. Mr. Gerald I. Evenden (USGS) and Mrs. Janet Fredericks (USGS) contributed suggestions regarding the computer programs essential to implement the analytical method presented here. Dr. Frank Manheim (USGS) provided critique and insight into the geologic and geochemical interpretations of the presented data. Mr. Lambert Montgomery (U.S. Bureau of Mines) kindly reviewed the manuscript.

4. GEOCHEMICAL ENRICHMENT VECTORS

The object of the geochemical enrichment vector analytical method (hereafter referred to as the "method") is to derive a single number for each analyzed sample in a study area such that the number represents the net enrichment of selected chemical components and is based upon coefficients derived from correlations of those components in a model. Coefficients correspond to weights, and the number, hereafter referred to as the net enrichment vector (NEV), corresponds to the sum of the weighted enrichments.

4.1 Enrichments

Geochemical enrichment is traditionally measured by the ratio of the concentration of an element in a sample to that of some standard concentration for that element such as crustal abundance or regional abundance. If the data value is greater than the value of the criterion,

the enrichment is greater than 1; if the data value is less than the criterion (*i.e.*, impoverished), the enrichment is less then 1 and greater than 0; if the data value equals the criterion, the enrichment is unity.

The method presented here treats geochemical analytical data transformed to enrichments in such a way that impoverishment is a negative number, enrichment is a positive number, and equality with the criterion is 0. This value is computed by subtracting 1 from the traditional enrichment ratio as shown below.

$$V = (v/K) - 1;$$

where:

V is the transformed data value
v is the original data value
K is the criterion with which v is compared.

4.2 **Weighted vectors**

The concept of geochemical enrichment vectors is predicated on the assumptions that for any given sample:

(1) enrichment of a variable can be expressed as a vector, and

(2) multiple enrichments compose a vector set whose resultant is the net enrichment of the sample.

Each datum transformed to an enrichment is a vector having both magnitude and direction. Magnitude is the numeric value of the enrichment; direction is the angular position of the vector relative to other vectors of the set. The angle between any two vectors in a set represents the correlation between them. Component vectors of a vector set share a common origin, and are in as many dimensions as there are component vectors.

When evaluating the NEV for a sample in a study area, contributing variables are weighted according to coefficients that reflect correlations between those variables in a model. If the variables are perfectly correlated, the vectors are coincident, and the angle between them is 0^{o}. If the variables are completely uncorrelated, the vectors are orthogonal. Therefore, the first step of the method is to establish the model from which one can quantify the correlations between selected variables and provide the coefficients necessary to weigh the enrichments of every sample in the study area.

After establishing a model, weights are computed by converting model area concentration data to enrichments and constructing a cross-product matrix of the enrichments. This matrix represents the correlations of all pairs of variables in the model area.

Next, by computing the 1st principal component of the cross-product matrix, a best-fit resultant vector is provided such that each term of the vector corresponds to the degree to which its corresponding variable contributes to the entire array. These terms are the desired model weights. Finally, terms of the 1st principal component are normalized so that the sum of their squared values is unity. The algorithm for computation of the cross-product matrix is shown below.

```
CVM = 0;
for( i=0; i < n; i++ )
        for( j=0; j < n; j++ ) CVM[i][j] += v[i] * v[j];

        where:
        CVM = the square cross-product matrix
        n = the order of CVM
        v = enrichment data value at a site
        i and j = indices to the variables
                  used in the computation
```

4.3 **Resultant vector**

After the weights are determined, they are applied to data in the study area. For each sample in the study area, each enrichment is multiplied by its corresponding model weight as determined in the model. The sum of these products is the value of the NEV. Weighting of the components of the vector set and computation of its final NEV are shown below.

```
E = 0;
for( i=0; i < n; i++ )
        E += v[i] * w[i] ;

where:
E = the final NEV
v[i] = an enrichment for the ith variable  at a site
w[i] = part of the 1st principal component
         associated with the ith variable.
```

4.4 **Example**

The following example utilizes raw concentrations, in percent, of Fe, Co, and Mn in manganese-rich samples derived from the Scripps Institute of Oceanography Sediment Data Bank (after McKelvey, et al., 1983). The geographic window from which these data were retrieved is in the Pacific Ocean, bounded by 20° N, 40° N, 140° E, and 160° E. Data are listed in Table 1., and the order of the records is preserved throughout the example.

TABLE 1. Original analytical data for manganese-rich samples.

lat	long	Mn	Fe	Co
21.483	159.538	21.600	16.300	.78000
24.027	159.450	22.600	14.800	.62000
23.815	159.437	18.550	13.600	.48000
26.200	153.730	16.330	15.770	.26000
29.522	153.407	17.700	9.9500	.32000
29.495	153.362	23.630	13.830	.66000
27.333	150.167	14.500	17.000	.19000
23.533	157.393	21.610	13.650	.64000
26.553	152.217	16.790	17.610	.47000
26.967	151.417	18.440	15.120	.34000
23.433	149.283	5.9000	12.900	.13000
28.383	148.250	23.730	15.730	.40000
27.933	147.650	17.200	8.9500	.11000
20.912	142.532	11.490	16.030	.09000
29.083	141.783	16.900	19.000	.22000
27.818	145.700	26.300	9.1300	.49000
31.725	157.500	11.500	13.300	.19000
31.850	157.333	7.2000	7.5000	.12000
31.905	157.137	18.400	15.300	.31000
31.683	156.450	14.000	8.1600	.10000
32.083	154.625	16.000	12.700	.12000
32.475	153.025	11.500	16.000	.10000
31.558	151.212	8.7000	2.9000	.17000
32.698	158.242	******	******	.48000
32.860	149.725	9.6800	16.940	.09000
32.018	149.273	19.050	16.150	.52000
32.383	148.425	11.150	16.250	.10000
36.483	146.717	1.9000	7.6000	******
38.000	146.000	19.800	13.900	.29000
38.467	146.000	20.430	16.190	.05000
38.017	145.983	16.600	15.350	.21000
34.010	145.945	16.550	18.350	.42000
34.137	144.187	16.400	20.000	.34000
36.028	143.412	7.1000	6.8100	.13000

Arithmetic means:
Mn = 15.7, Fe = 13.7, Co = 0.3

(****** indicates missing data)

The entire data set, *per se*, was used as the model for computation of weights in this example. Table 2 is a copy of the output of the vector analysis computer program that shows the cross-product matrix and the weights derived from it. Note that two records had missing data and could not be used in the computation.

TABLE 2. Product matrix and corresponding weights.

Product matrix

	Mn	Fe	Co
Mn	3.437518	0.832485	4.904182
Fe	0.832485	2.513719	1.274282
Co	4.904182	1.274282	13.762219

Weights

Mn	Fe	Co
0.370668	0.110940	0.922116

Of 34 input records, 2 were flagged because of missing data.

The original concentrations of Mn, Fe, Co, and the NEV for combined Mn, Fe, and Co in each record are shown in Table 3.

TABLE 3. Concentrations and corresponding NEV of Mn, Fe, and Co

lat	long	Mn	Fe	Co	Enrichment
21.483	159.538	21.600	16.300	.78000	1.635735
24.027	159.450	22.600	14.800	.62000	1.155403
23.815	159.437	18.550	13.600	.48000	0.619747
26.200	153.730	16.330	15.770	.26000	-0.091312
29.522	153.407	17.700	9.9500	.32000	0.078327
29.495	153.362	23.630	13.830	.66000	1.294814
27.333	150.167	14.500	17.000	.19000	-0.339718
23.533	157.393	21.610	13.650	.64000	1.184191
26.553	152.217	16.790	17.610	.47000	0.579929
26.967	151.417	18.440	15.120	.34000	0.199137
23.433	149.283	5.9000	12.900	.13000	-0.760383
28.383	148.250	23.730	15.730	.40000	0.513394
27.933	147.650	17.200	8.9500	.11000	-0.587057
20.912	142.532	11.490	16.030	.09000	-0.726009
29.083	141.783	16.900	19.000	.22000	-0.174648
27.818	145.700	26.300	9.1300	.49000	0.797260
31.725	157.500	11.500	13.300	.19000	-0.440508
31.850	157.333	7.2000	7.5000	.12000	-0.804156
31.905	157.137	18.400	15.300	.31000	0.107439
31.683	156.450	14.000	8.1600	.10000	-0.699742
32.083	154.625	16.000	12.700	.12000	-0.554285
32.475	153.025	11.500	16.000	.10000	-0.695279
31.558	151.212	8.7000	2.9000	.17000	-0.652306
32.698	158.242	******	******	.48000	******
32.860	149.725	9.6800	16.940	.09000	-0.761373
32.018	149.273	19.050	16.150	.52000	0.775149
32.383	148.425	11.150	16.250	.10000	-0.701517
36.483	146.717	1.9000	7.60000	******	******
38.000	146.000	19.800	13.900	.29000	0.067681
38.467	146.000	20.430	16.190	.05000	-0.636594
38.017	145.983	16.600	15.350	.21000	-0.242025
34.010	145.945	16.550	18.350	.42000	0.426569
34.137	144.187	16.400	20.000	.34000	0.190491
36.028	143.412	7.1000	6.81000	.13000	-0.781367

5. DATA DESCRIPTION

A northern Pacific Ocean subset of the Scripps Institution of Oceanography's Sediment Data Bank was used to test the design and implementation of the method. The area of the northern Pacific Ocean was subdivided into fourteen 20^{o} X 20^{o} geographic subregions within the area bounded by 0^{o} N., 40^{o} N., 120^{o} E., and 100^{o} W (Fig. 13). Data from approximately 1200 Mn-rich samples were then grouped according to their respective 20^{o} subregions.

Each record of the subset represents one sample and contains positional coordinates, depth of sample, and concentrations of cobalt, nickel, and manganese. These elements were arbitrarily selected because they are well known as major components of both crusts and nodules, thereby providing prior knowledge as a correlative frame of reference. Other variables present in the master data bank were not used in this study.

6. PRELIMINARY DATA ANALYSIS

Before transformation to enrichments, Co, Ni, and Mn were analyzed statistically to determine their frequency and correlation attributes which are essential to the vector computations as well as subsequent NEV interpretation.

6.1 Frequency analysis

Histograms and ogives were computed for all variables in each subregion and for all subregions considered collectively. The principal parameters derived from these distributions are the mean, variance and standard deviation, median, high and low extreme data values, and various percentile ranges. Sturges' Rule (after Huntsberger, 1963, p. 10) was used to define the number of classes in each distribution. Tables 4, 5, and 6 summarize the frequency data. Subregion 0 is omitted because of insufficient and/or questionable data values.

TABLE 4. Descriptive statistics for Co in 13 northern Pacific subregions.

Sub-region	Number of Samples	Percent* Min	Median	Max	IQR
01	33	.05	.25	.78	.35
02	40	.04	.33	1.04	.25
03	50	.07	.26	1.64	.19
04	52	.01	.28	1.17	.20
05	39	.01	.19	.90	.18
06	89	.01	.11	1.00	.07
07	63	.01	.12	1.10	.12
08	139	.05	.24	.70	.10
09	367	.03	.21	.58	.08
10	219	.03	.27	1.34	.16
11	22	.09	.42	1.50	.43
12	20	.01	.32	.51	.18
13	26	.03	.24	.54	.15
all	1159	.01	.22	1.64	.14

* Min, Max, IQR = data minimum, maximum and inter-quartile range, respectively.

TABLE 5. Descriptive statistics for Ni in 13 northern Pacific subregions.:

Sub-region	Number of Samples	Percent* Min	Median	Max	IQR
01	33	.07	.33	1.16	.25
02	40	.09	.46	.97	.23
03	50	.10	.46	1.15	.37
04	56	.01	.44	1.36	.33
05	40	.03	.57	1.45	.46
06	127	.05	1.00	1.69	.25
07	67	.04	.95	1.89	.76
08	148	.11	1.20	1.95	.26
09	370	.15	1.10	1.74	.44
10	219	.08	.59	1.54	.42
11	22	.28	.52	1.17	.37
12	20	.03	.34	1.17	.19
13	28	.03	.28	1.30	.20
all	1220	.01	.93	1.95	.72

* Min, Max, IQR = data minimum, maximum and inter-quartile range, respectively.

TABLE 6. Descriptive statistics for Mn in 13 northern Pacific subregions.

Sub-region	Number of Samples	Percent* Min	Median	Max	IQR
01	33	1.9	16	26.2	7.5
02	40	2.2	19	25.7	5.2
03	50	6.7	18	36.7	5.6
04	57	0.1	16	28.0	8.2
05	40	0.6	16	27.0	8.5
06	127	11.7	25	39.5	2.6
07	65	1.7	25	45.5	10.5
08	144	2.5	26	37.5	4.9
09	365	2.6	23	36.4	6.8
10	219	1.9	19	34.2	5.2
11	22	10.8	18	50.2	6.8
12	20	5.0	14	27.2	6.3
13	28	.07	15	32.5	5.2
all	1210	.07	22	50.2	8.8

* Min, Max, IQR = data minimum, maximum and inter-quartile range, respectively.

Cumulative frequency statistics for each variable in all subregions are summarized in Figures 1, 2 and 3. In each figure the subregion ogives for that variable are collectively plotted on a single graph that is scaled to the data extremes of that variable in the entire region. Then, for the entire range of cumulative frequencies, the area bounded by highest and lowest data values is shaded-in resulting in a graphic that could be considered a cumulative frequency distribution signature for the entire study area.

The frequency distribution signatures for both Mn and Ni are similarly shaped and show a rather constrained range of enrichments below cumulative frequencies of 80 percent. As expected, most enrichments are low, and very few are high. Co, on the other hand, shows a significant increase in enrichment throughout the full range of increasing cumulative frequency. A comparison of Figures 1, 2, and 3, clearly shows that the aggregated cumulative frequency distribution signature for Co is completely different than that of either Mn or Ni.

6.2 **Correlation analysis**

As a preliminary measure of the correlations between variables, Pearson product-moment linear correlation coefficients were computed for all pairs of variables. No attempt was made to transform or normalize the data. The correlation computation was executed as a rough first pass effort to identify the strongest correlations in the original analytical data. Table 7 lists the correlation coefficients calculated for the

element pairs Co-Ni, Ni-Mn and Co-Mn. Statistics are provided for each subregion and for all subregions considered collectively.

TABLE 7. Correlation statistics for Co, Ni and Mn in 13 northern Pacific subregions.

Sub-region	Correlation Coefficients Co-Ni	Ni-Mn	Co-Mn	Valid pairs Co-Ni	Ni-Mn	Co-Mn
1	.58	.71	.71	32	33	32
2	.05	.65	.63	40	40	40
3	-.16	.46	.62	50	50	50
4	-.0	.47	.72	52	56	52
5	.21	.65	.53	39	40	39
6	-.16	.30	-.26	89	127	89
7	.15	.65	.33	63	65	61
8	.15	.75	.15	145	150	141
9	-.13	.74	-.04	361	359	356
10	-.34	.73	.05	219	219	219
11	.17	.45	.73	22	22	22
12	.38	.50	.74	20	20	20
13	.01	.79	.23	26	28	26
all	-.18	.71	.11	1158	1209	1147

Table 7 shows that the Co-Ni pair is essentially uncorrelated in all subregions except for subregion 01. This broad spatial distribution of low correlations implies a pervasive geologic environment in which Ni and Co are independent. Subregion 01 contains the Bonin-Ogasawara arc, which is, in part, the site of hydrothermal activity (Usui, *et al.*, 1986) that may account for the local high correlation between Co and Ni. Figure 10 shows the spatial distribution of the correlation coefficients for the Co-Ni pair.

Figures 11 and 12 are spatial distributions of the Ni-Mn and Co-Mn correlation coefficients in their respective subregions. The Ni-Mn plot shows a distinct zone of low correlations that trends diagonally across the area from northeast to southwest. Co-Mn correlations are dramatically reduced in the southeast corner of the region in areas of known high density of abyssal manganese nodules.

6.3 **Scatter plots**

After original weight-percent data have been transformed to enrichments, scatter plots were generated for all variable pairs and for depth versus each variable.

Plots of enrichments for the pairs Mn-Co (Fig. 4), Co-Ni (Fig. 5), and Mn-Ni (Fig. 6) show no visibly distinctive patterns that might suggest

data partitions on the basis of either enrichment or frequency. This is not the case when sample depth is plotted versus enrichment of Co, Ni, and Mn (Figures 7, 8, and 9). In each of these cases there are two moderately well defined clusters of analytical data; one major cluster below and one minor cluster above a sample depth of about 3000 meters. This indicates a strong sampling depth bias in favor of deep samples.

7. DATA PORTRAYAL

Cartographic display is an inescapable requisite when dealing with spatially dependent data and, in this regard, there are some manipulations performed on the enrichment data in this report that have significant effect on the data distribution. Gridding and contouring usually modify the data surface by smoothing it for aesthetic reasons and (or) to estimate values in areas barren of data. The following is a brief account of the data treatment following transformation to enrichment and prior to display as a graphic document.

7.1 Gridding and interpolation

After repeated trial and consideration of various gridding parameters, a grid mesh size of 77 columns by 28 rows with a search radius of 5 mesh units was selected to accommodate the North Pacific data window from 0^{o} to 40^{o} N. and 120^{o} E. to 100^{o} W. Data are interpolated using a function that approximates inverse squared distance (Evenden, 1986 (b)).

7.2 Contouring

After gridding, data are portrayed as contour maps with a contour interval of 0.1 units of enrichment. Contour lines were smoothed by a spline function (Evenden, 1986 (a)) and, to avoid surface artifacts due to forced closure, lines were truncated against areas void of data, including map margins.

7.3 Overlays

Three transparent overlays accompany the set of seven enrichment vector maps found in the pocket at the end of the report: Coastlines, sample sites, and 20^{o} subregion boundaries (Fig. 13); Sample depths (Fig. 14); 200-mile limit (Fig. 15).

Depth-of-sample data were gridded using the same parameters used for the enrichment data (*cf.* Section 7.1). Also, one must keep in mind that the depth-of-sample surface in this report is not appropriate for bathymetry. Sample depth defines only the relief associated with the geochemical landscape, not the topography.

8. GEOCHEMICAL ENRICHMENTS OF NORTHERN PACIFIC MANGANESE OXIDE PHASES

Sample data were transformed to enrichments using the medians of those variables in their host subregions as the criteria (denominators) for the transformations. For NEV analysis each subregion was considered a model, and a cross-product matrix was computed for each. The terms of the first principal component of each cross-product matrix were used as weights in subsequent NEV computations for data in their respective subregions.

The following NEV maps are the result of the method applied to Mn oxide phase data from the northern Pacific: Cobalt Enrichment (Fig. 16), Nickel Enrichment (Fig. 17), Manganese Enrichment (Fig. 18), Cobalt-Manganese Enrichment (Fig. 19), Nickel-Manganese Enrichment (Fig. 20), Cobalt-Nickel Enrichment (Fig. 21), and Cobalt-Nickel-Manganese Enrichment (Fig. 22). Red contours signify positive NEV's on all of the above maps. The following is a discussion of the salient features of each of them.

The reader should note that subregions 00, 11 and 12 have a very low sample density, and their contribution to the overall picture should be regarded with caution pending verification by additional data.

8.1 **Cobalt enrichment**

Figure 16 is a plot of the Co NEV surface for the entire study area. There are two areas of high enrichment: (1) a broad east-west band that includes most of subregions 00, 01, 02, 03, 10, 11, 12, and 13, and (2) a smaller area that occupies most of subregions 05 and 06 immediately adjacent to the western coast of Baja California. The highest enrichments of the study area are in subregion 11.

The high enrichment of Co in subregion 06 may be an artifact caused by the inclusion of very low grade Co samples captured from an area of hydrothermal activity (F.T. Manheim, 1987, personal communication). Including low concentration data in the subregion population reduces the median and, for a given concentration, increases the enrichment. This could have a profound effect on enrichments computed using weights derived from these data. As shown in Table 4, the median and interquartile range for Co in subregion 06 are the lowest in the entire study area. For future work it is probably best to consider this subregion apart from other subregions, and to calculate weights using other criteria.

8.2 **Nickel enrichment**

Figure 17 is a plot of the Ni NEV surface for the entire study area. High Ni enrichment forms two almost-complete halos that approximately encircle low-enrichment areas at the junctions of subregions 00, 01, 12, 13, and 03, 04, 09, and 10. When viewed together with the sample-site-distribution and depth-of-sample overlays (Figs. 13 and 14), it is

readily apparent that the high Ni enrichment occurs in the deep areas of the geochemical landscape.

8.3 **Manganese enrichment**

Figure 18 is a plot of the Mn NEV surface for the entire study area. The apparent low range of Mn enrichments is because it is a major chemical component of the samples, and its metric is approximately two orders of magnitude greater than those of either Ni or Co. Mn enrichment is highest in subregion 11.

8.4 **Nickel-cobalt enrichment**

Figure 21 is a plot of the Ni-Co NEV surface for the entire study area. The very strong influence of Co enrichment overpowers the effect of its combination with Ni, and the distribution is quite similar to that of Co alone (Figure 16).

One area of minor difference between Co enrichment and that of the Ni-Co pair is located in the southeastern part of subregion 01. What appears as a slightly enriched saddle for Co enrichment is resolved as a more continuous zone of distinctly higher enrichment for the Ni-Co pair. Comparison of Ni-Co with Ni (Fig. 17) shows that the area of high Co enrichment in the southeastern part of subregion 01 coincides with a strong high Ni enrichment.

Other than the high Ni enrichment in subregion 01, enrichment of Ni and Ni-Co have very little in common.

8.5 **Cobalt-manganese enrichment**

Figure 19 is a plot of the Co-Mn NEV surface for the entire study area. Distribution of Co-Mn enrichments is essentially identical to that of Co.

8.6 **Nickel-manganese enrichment**

Figure 20 is a plot of the Ni-Mn NEV surface for the entire study area. Almost all of the high enrichments are directly correlated with the deep (*i.e.*, high depth of sample) parts of the study area. One small positive enrichment area is situated in subregion 05. The major area of high enrichment in the study area forms a semicontinuous zone encircling two separate zones of low enrichment centered at the junctions of subregions 00, 01, 12, 13, and 03, 04, 09, 10. Except for some very minor shifts and slight changes in continuity of the enrichment surfaces, the distribution of Ni-Mn is almost identical to that of Ni.

8.7 **Cobalt-nickel-manganese enrichment**

Figure 22 is a plot of the Co-Ni-Mn NEV surface for the entire study area. The NEV surface for this trio of elements is almost identical to that of Co.

9. **CONCLUSIONS**

The NEV maps show areas that are enriched with respect to Co, Ni and Mn, and combinations thereof, and draw attention to many specific zones of the study area. The most interesting of these include subregions 11, 05, 06, and 00 where, unfortunately, many of the exceptionally high enrichments occur in areas truncated by the map or in areas of low sample density. A next step would be to acquire and analyze additional data in these areas. Analysis at larger scales may show many features lost in the broad-brush approach used here.

It is not so much the purpose of this report to pursue the enrichment characteristics within the study area as it is to demonstrate the viability and credibility of the presented method of data analysis.

9.1 **Credibility**

In its simplest application, the geochemical enrichment vector analytical method deals with distributions of elements. To this end, it is reassuring to find some agreement between the results gained by the new method and preexisting observations or analyses. Many of the major zones of high enrichment designated in this report agree with areas of high elemental concentrations previously determined in other studies (McKelvey, 1986; Cronan, 1980), thus ensuring concordance with some published observations of others.

9.2 **Sensitivity**

Because the entire method is driven by a model, it is sensitive to changes in model parameters such as the selection of variables and definition of model areas. For example, some distributions of enrichments of trace elements computed by using the arithmetic mean may be significantly different from those computed by using the median.

To date, experience with the method has shown that inconsistencies within the data set being analyzed are more likely to cause misinterpretations than any failing of the method. By design, the method computes weights and NEV's, and it is blind to inconsistencies in the data. It is of special importance that the user be well informed about the source database attributes, including such things as the significance of numeric data, the exact definition of a unit record, the chemical analytical methods used, and the accuracy of sample descriptions.

9.3 **Additional support**

To explain fully the nature of the variables that compose both the model area and the study area, the presented method should be undertaken in parallel with conventional statistical analysis. For example, the spatial distribution of correlation coefficients proved to be valuable geologic descriptors even though they are not an intrinsic part of the method. The tables summarizing frequency statistics helped to explain features such as the Co enrichment of subregion 06 which otherwise might be misinterpreted.

It is this writer's opinion that statistical data analysis is a requisite to enrichment vector analysis. Of particular importance is the use of statistics to define the attributes of both model and study areas, thus helping to select a sound framework within which the method can function.

9.4 **Future development**

Based upon the observed variety of NEV ranges, it appears that scaling factors might be necessary to equate them in some cases. In addition to the scaling of the variables, it would be advantageous to derive a discriminant function that will accept or reject inclusion of a variable in a vector set. These aspects of geochemical enrichment vectors will receive attention in the very near future.

From a geological standpoint, the data used for the analysis in this report have shown that there may be very distinct partitions that can be made on the basis of concentration criteria. Dividing data into various populations according to chemistry will add depth and scope to future analyses.

Major near-future goals in method development are manipulation and portrayal of data and data transformations in image form. Image processing techniques will be designed to utilize various data filters to show clearly multivariate data attributes that are not nearly as visible when portrayed by conventional cartographic methods.

10. **REFERENCES**

Cronan, D.S., 1980, Underwater minerals: Academic Press, New York, 362 p.

Evenden, G.I., 1986 (a), CONTOUR: Unpublished administrative report, U.S. Geological Survey Computer Program Library, Woods Hole, MA.

---- 1986 (b), GRIDS: Unpublished administrative report, U.S. Geological Survey Computer Program Library, Woods Hole, MA.

Glasby, G.P., 1972, The mineralogy of manganese nodules from a range of marine environments: Marine Geology, v. 13, p. 57-72.

Halbach, P., Scherhag, C., Hebisch, U., Marchig, V., 1981, Geochemical and mineralogical control of different genetic types of deep-sea nodules from the Pacific ocean: Mineral Deposita, v. 16, p. 59-84.

Huntsberger, D.V., 1963, Elementary statistics: Allyn and Bacon, New York, 291 p.

Johnson, C.J., Clark, A.L., 1985, Potential of Pacific ocean nodule, crust, and sulfide mineral deposits: Natural Resources Forum, v. 9, n. 3, p. 179-186.

McKelvey, V.E., 1986, Subsea mineral resources: U.S. Geological Survey Bulletin 1689-A, 106 p.

McKelvey, V.E., Wright, N.A., Bowen, R.W., 1983, Analysis of the world distribution of metal-rich subsea manganese nodules: U.S. Geological Survey Circular 886, 55 p.

Usui, A., Yuasa, M., Yokota, S., Nohara, M., Nishimura, A., Murakami, F., 1986, Submarine hydrothermal manganese deposits from the Ogasawara (Bonin) arc, off the Japan islands: Marine Geology, v. 763, p. 311-332.

Figure 1. Aggregated Ogives for Cobalt

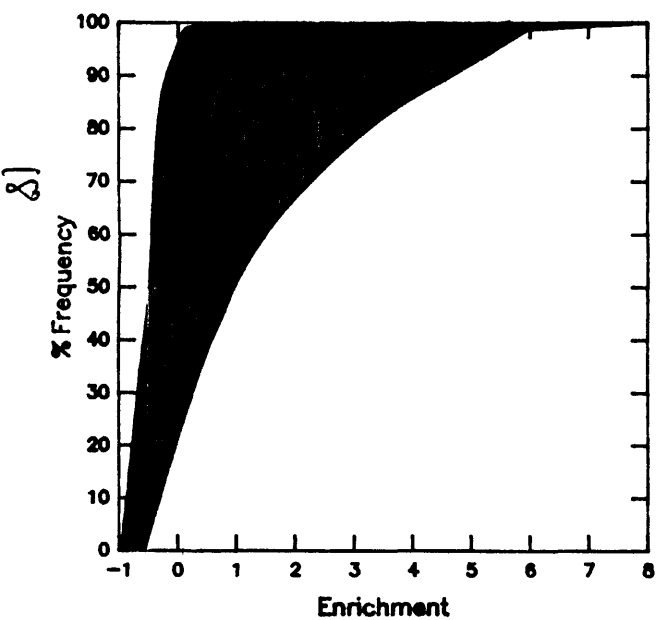

Figure 2. Aggregated Ogives for Nickel

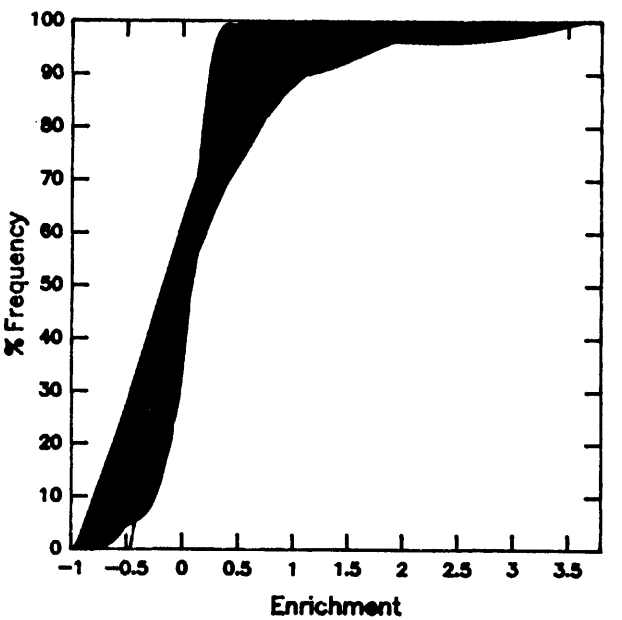

Figure 3. Aggregated Ogives for Manganese

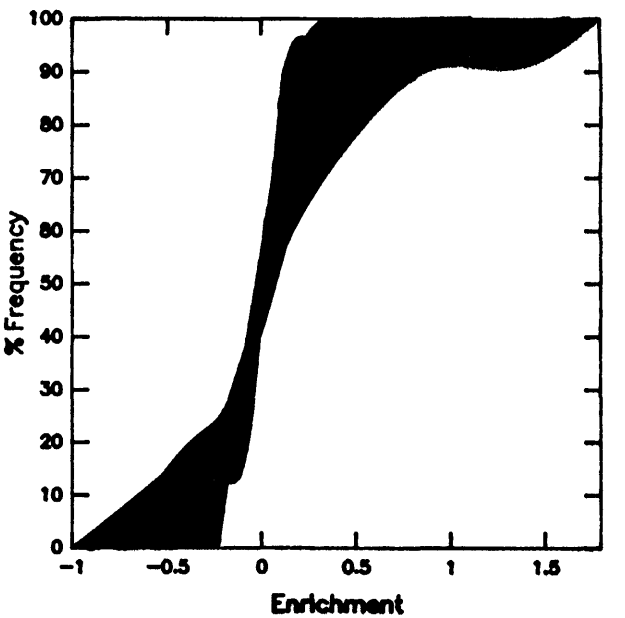

Figure 4. Scatter Plot of Manganese vs Cobalt

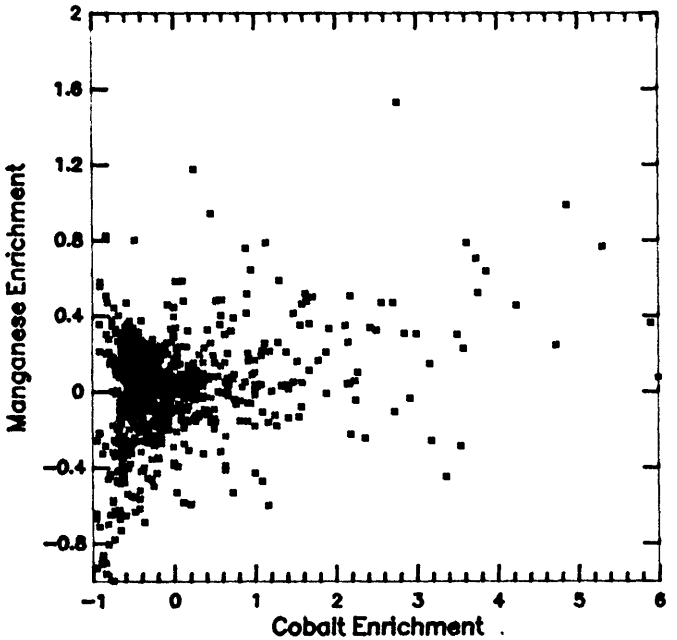

Figure 5. Scatter Plot of Cobalt vs Nickel

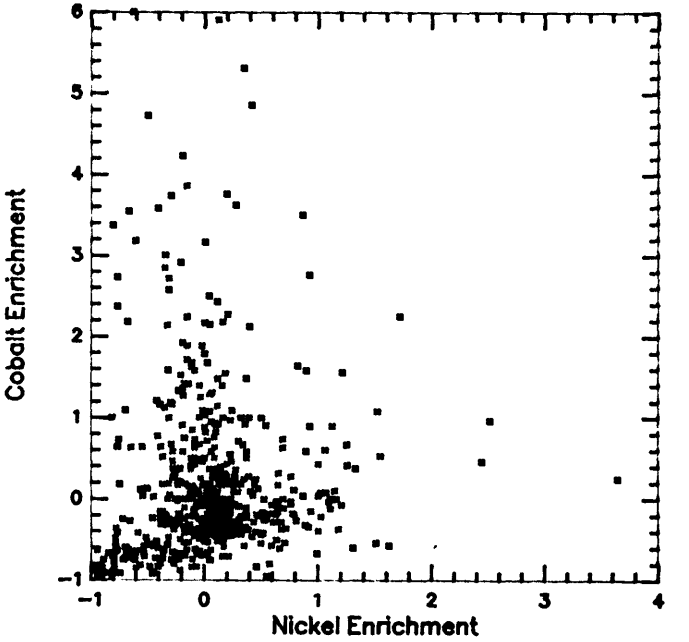

Figure 6. Scatter Plot of Manganese vs Nickel

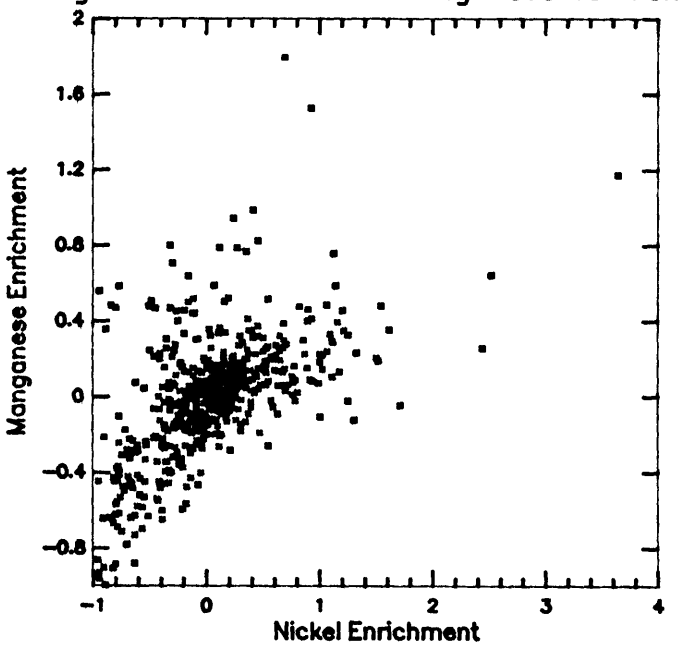

Figure 7. Scatter Plot of Depth vs Cobalt

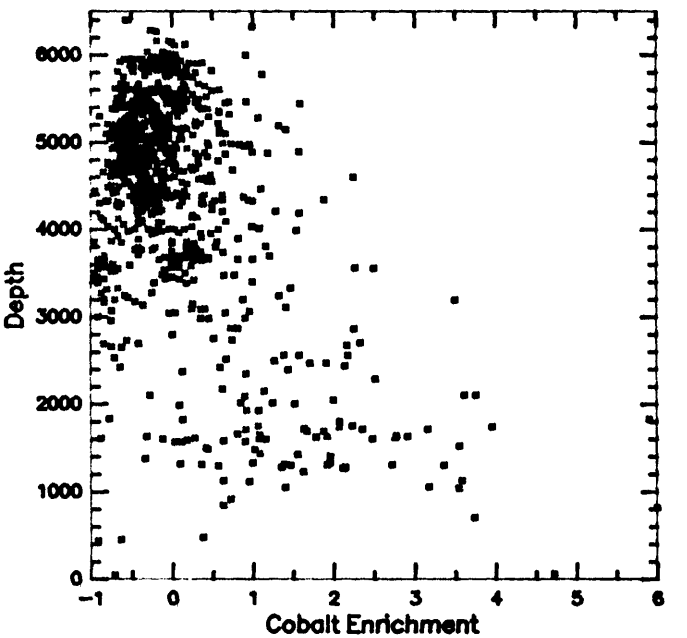

Figure 8. Scatter Plot of Depth vs Nickel

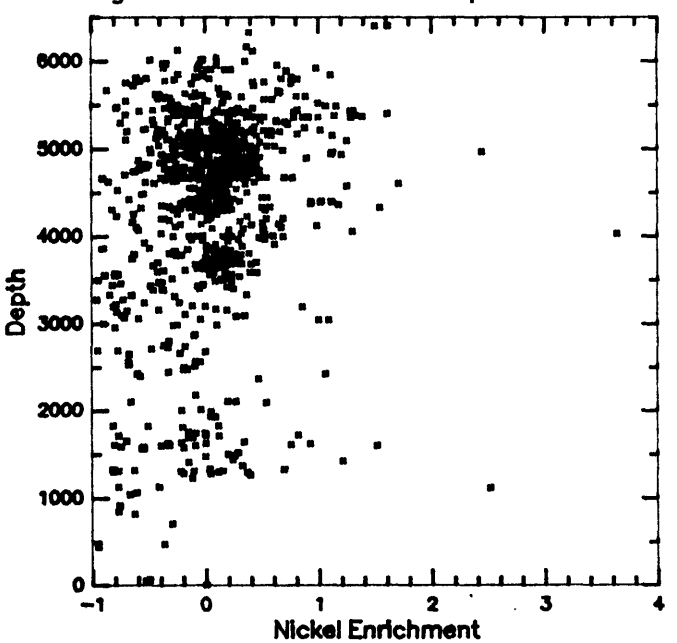

Figure 9. Scatter Plot of Depth vs Manganese

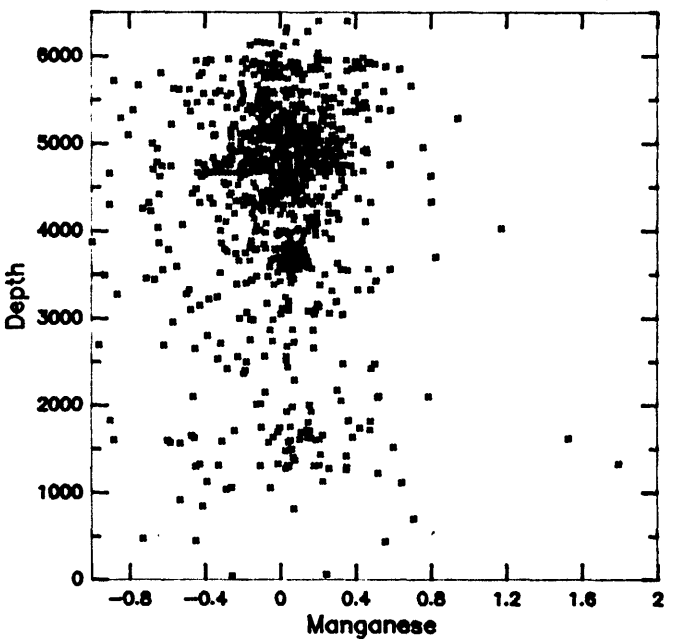

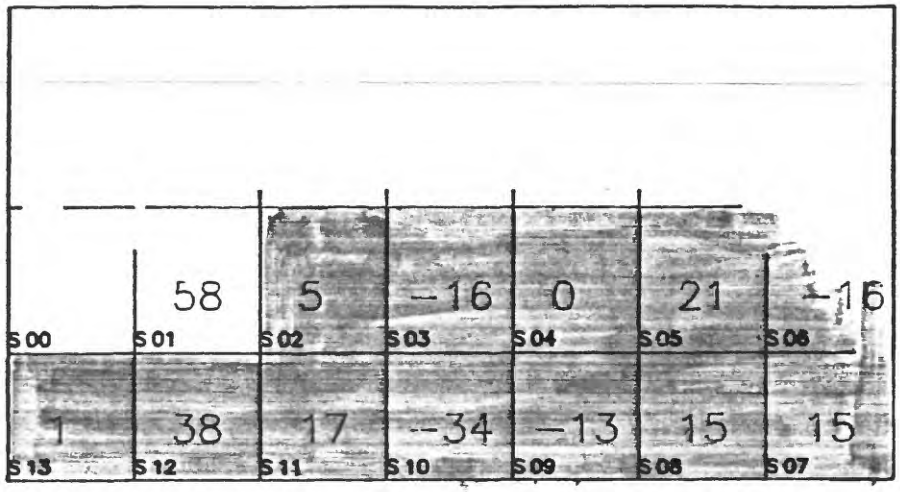

Figure 10. Co–Ni Correlation Coefficients (X 100)

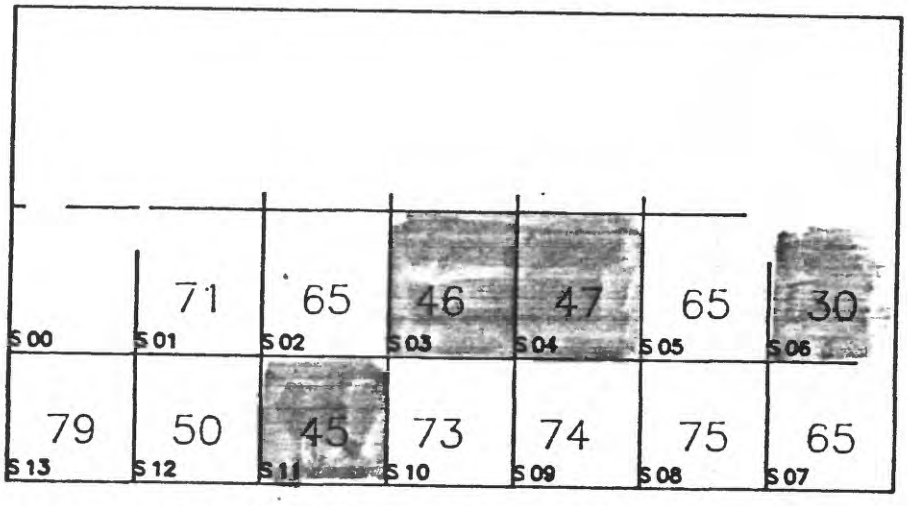

Figure 11. Ni–Mn Correlation Coefficients (X 100)

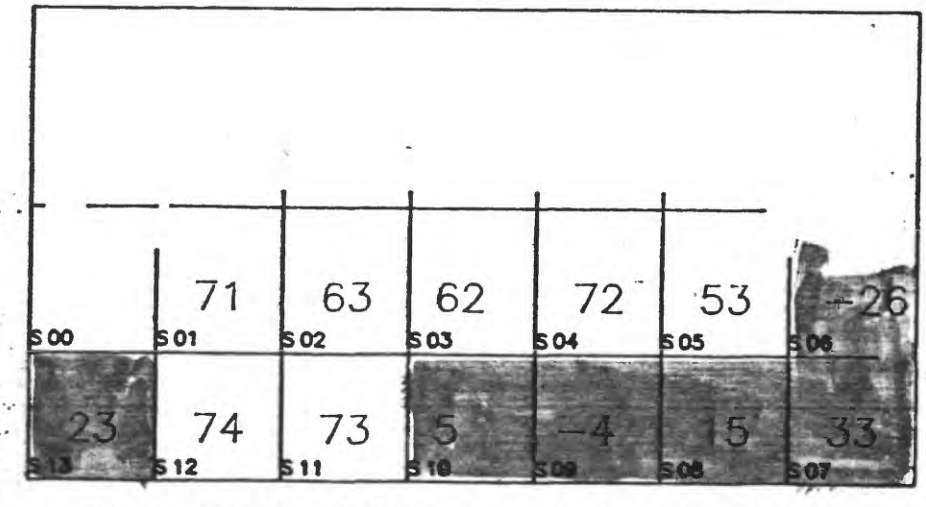

Figure 12. Co–Mn Correlation Coefficients (X 100)

Figure 13. Coastlines, sample sites, and 20° sub-regions of the northern Pacific study-area

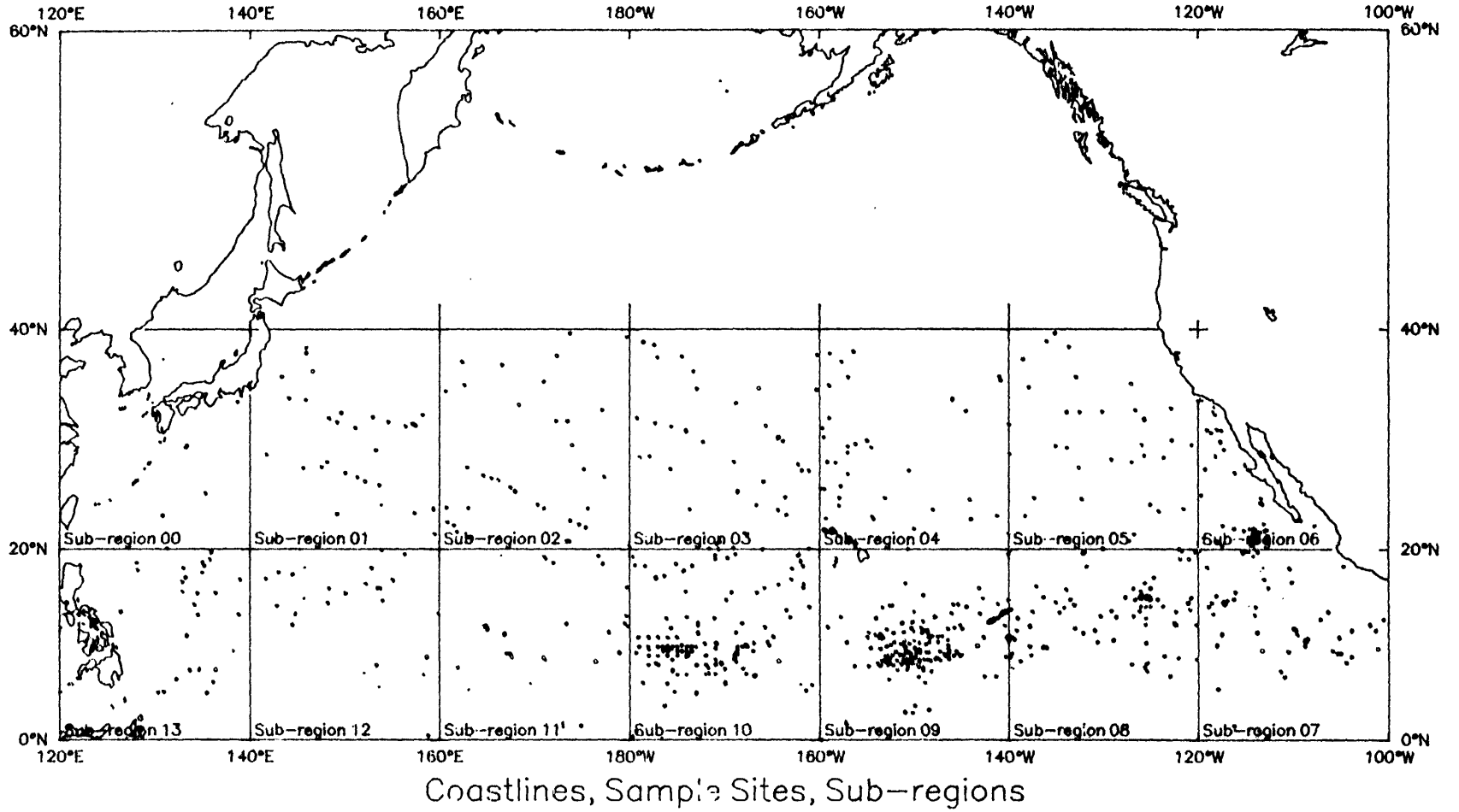

Figure 14. Depths of samples in the northern Pacific study-area

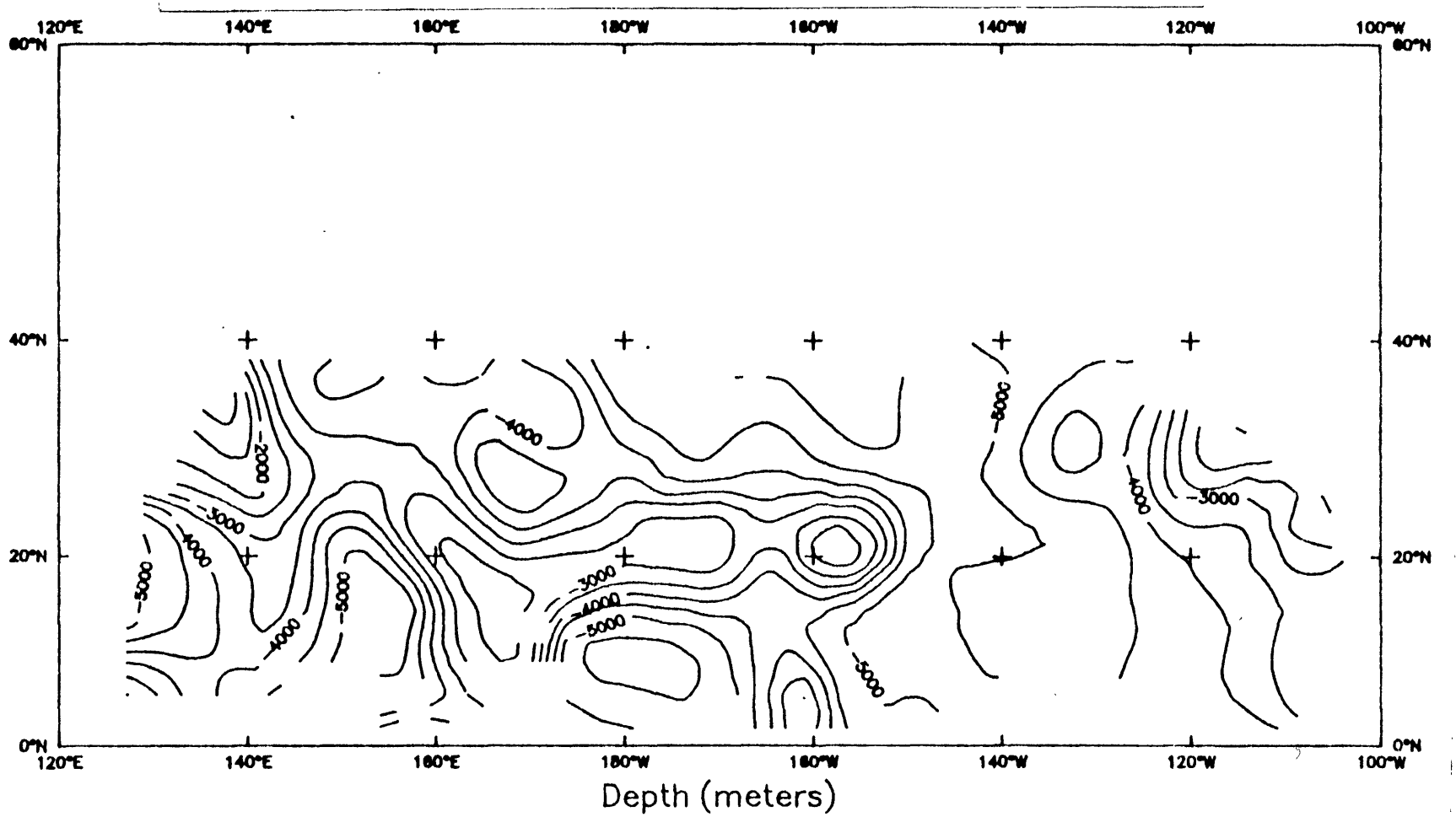

Figure 15. 200 mile offshore boundaries within the northern Pacific study-area

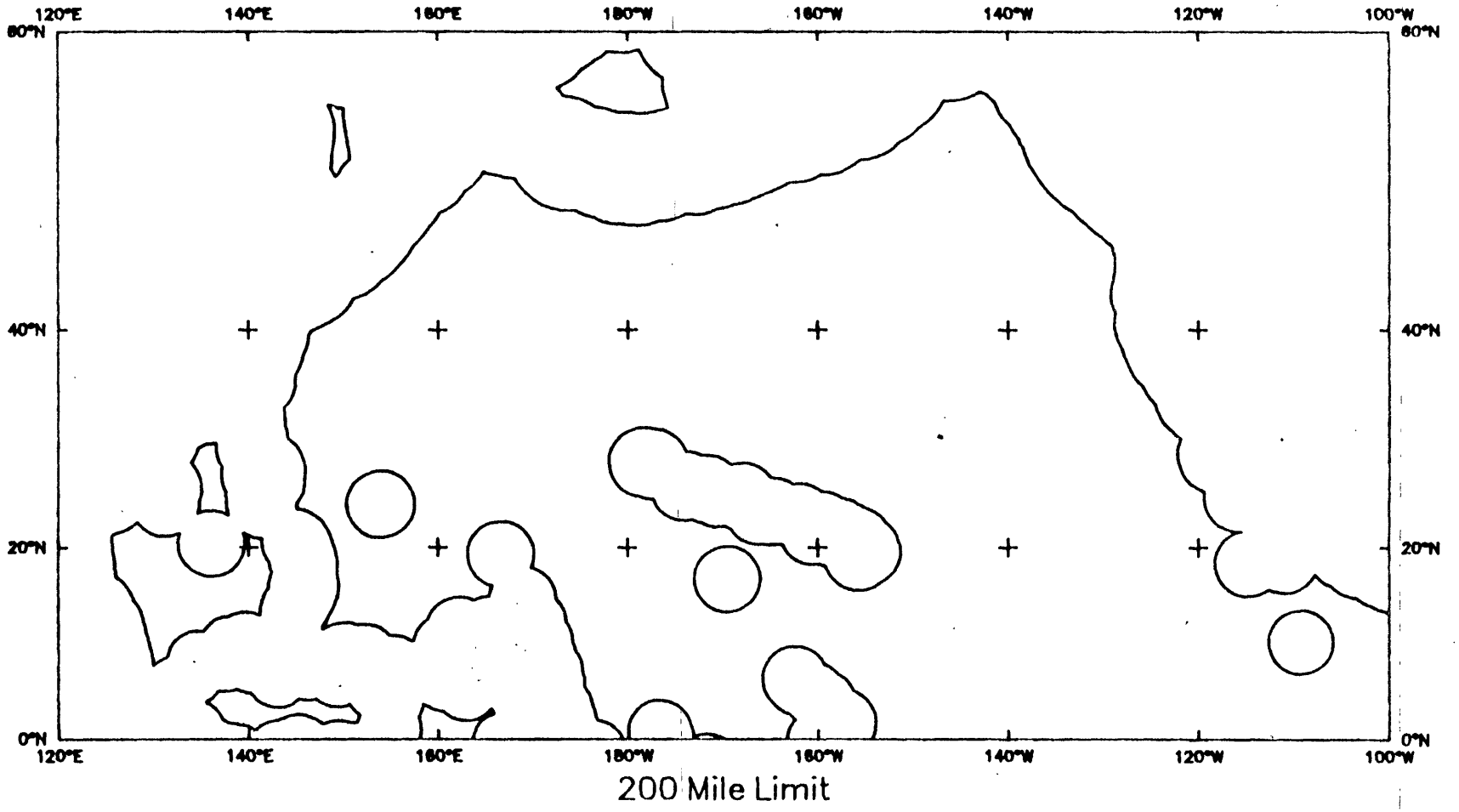

Figure 16. Distribution of Co enrichment in the northern Pacific study area

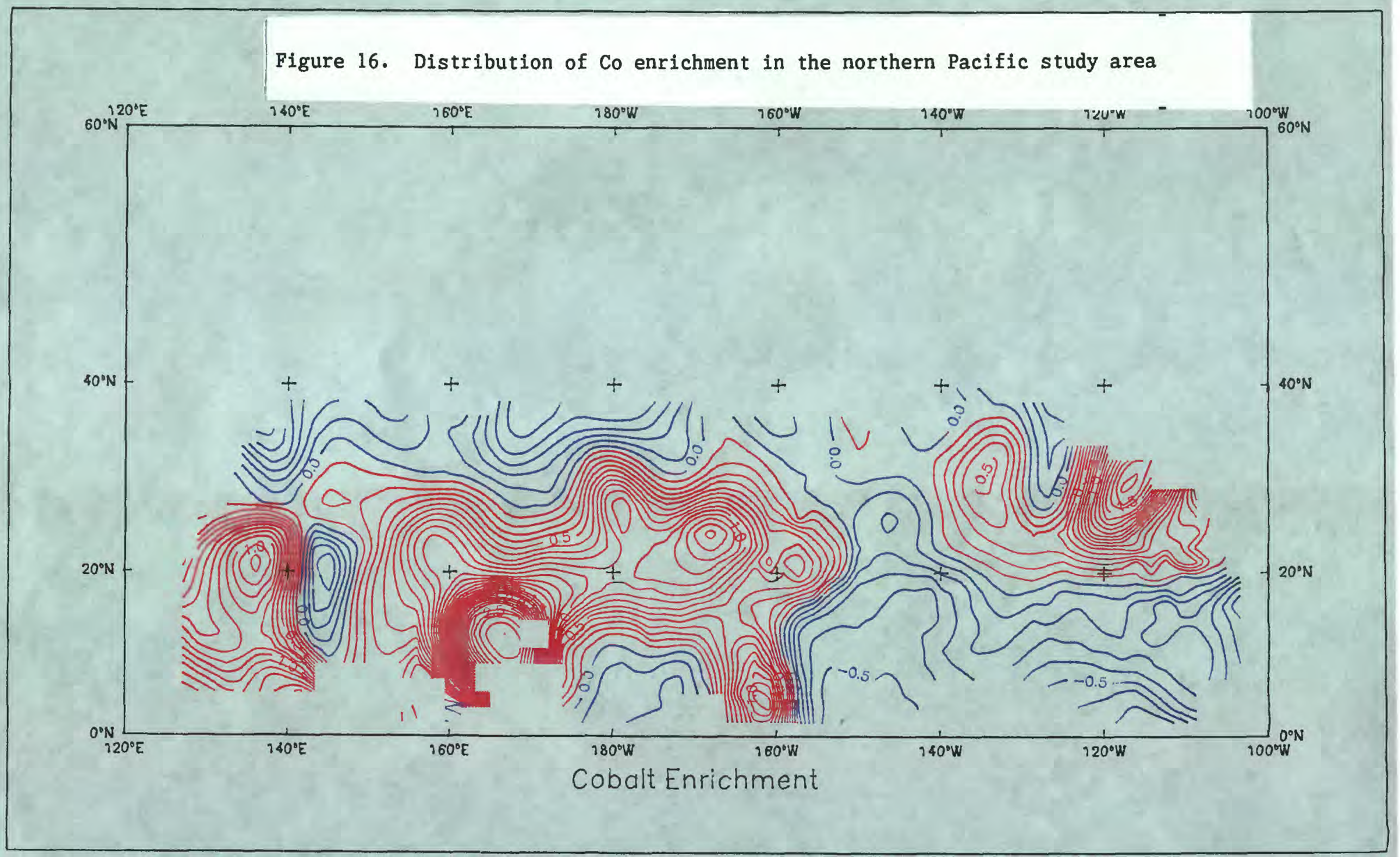

Figure 17. Distribution of Ni enrichment in the northern Pacific study area

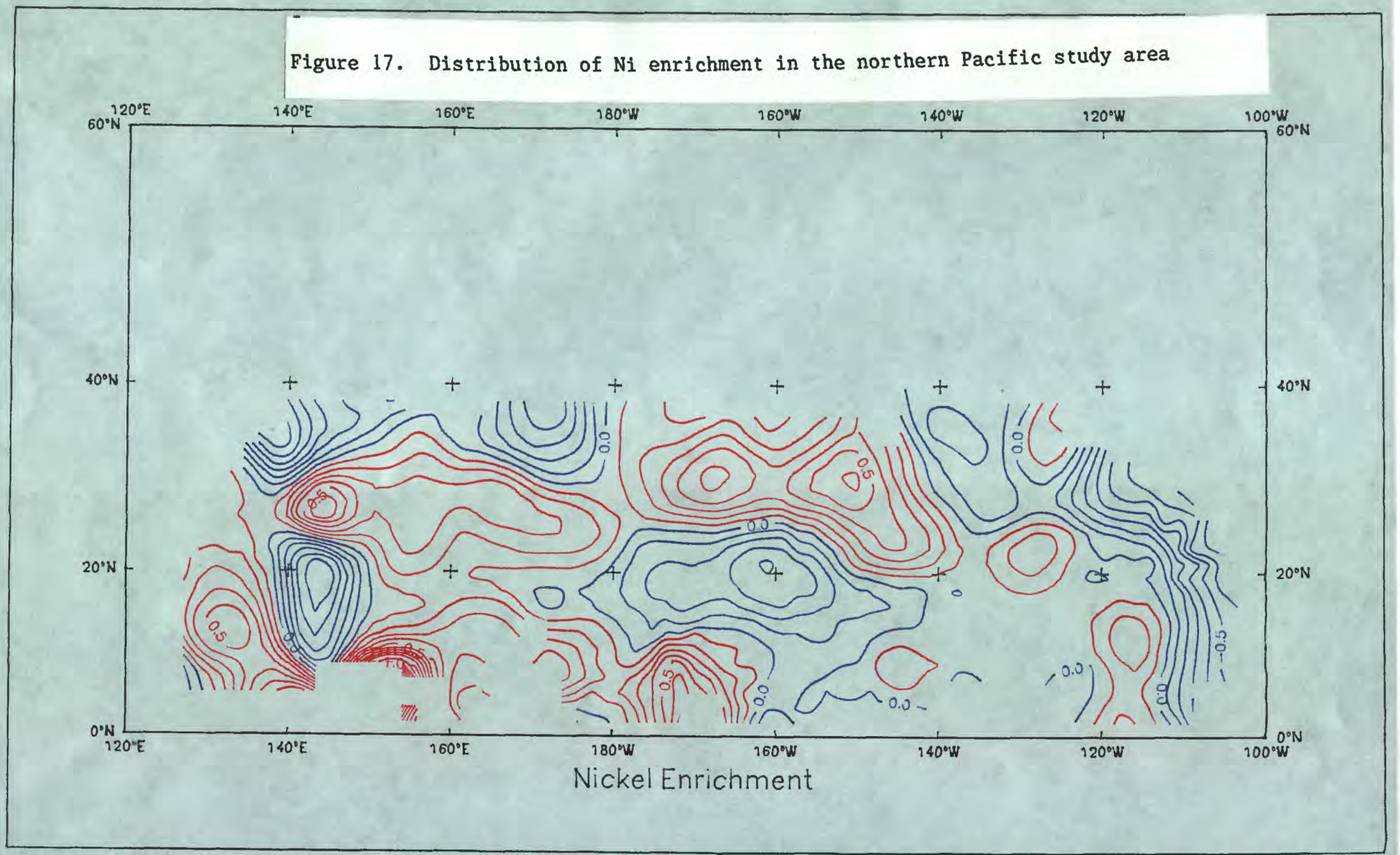

Figure 18. Distribution of Mn enrichment in the northern Pacific study area

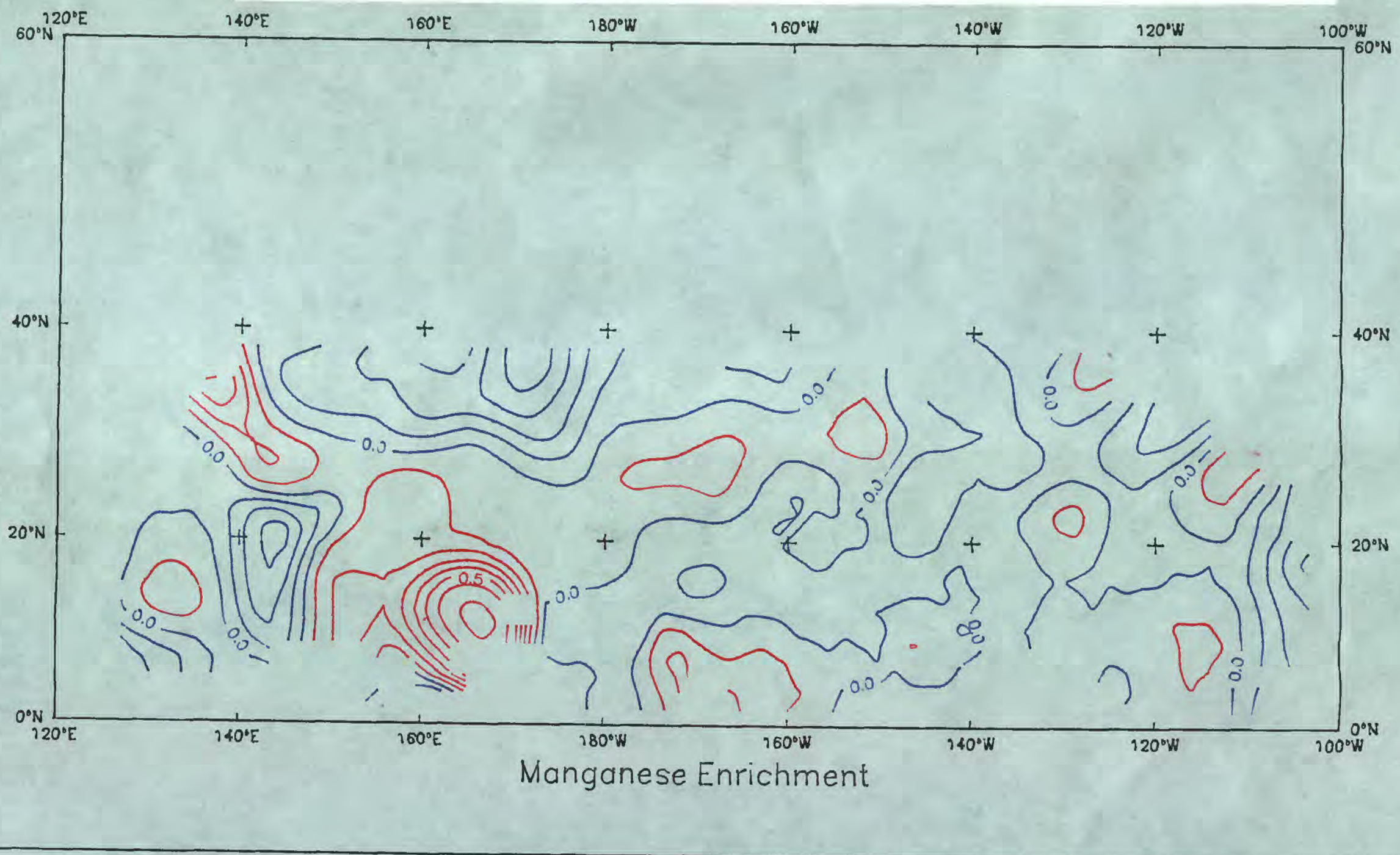

Figure 19. Distribution of Co-Mn enrichment in the northern Pacific study area

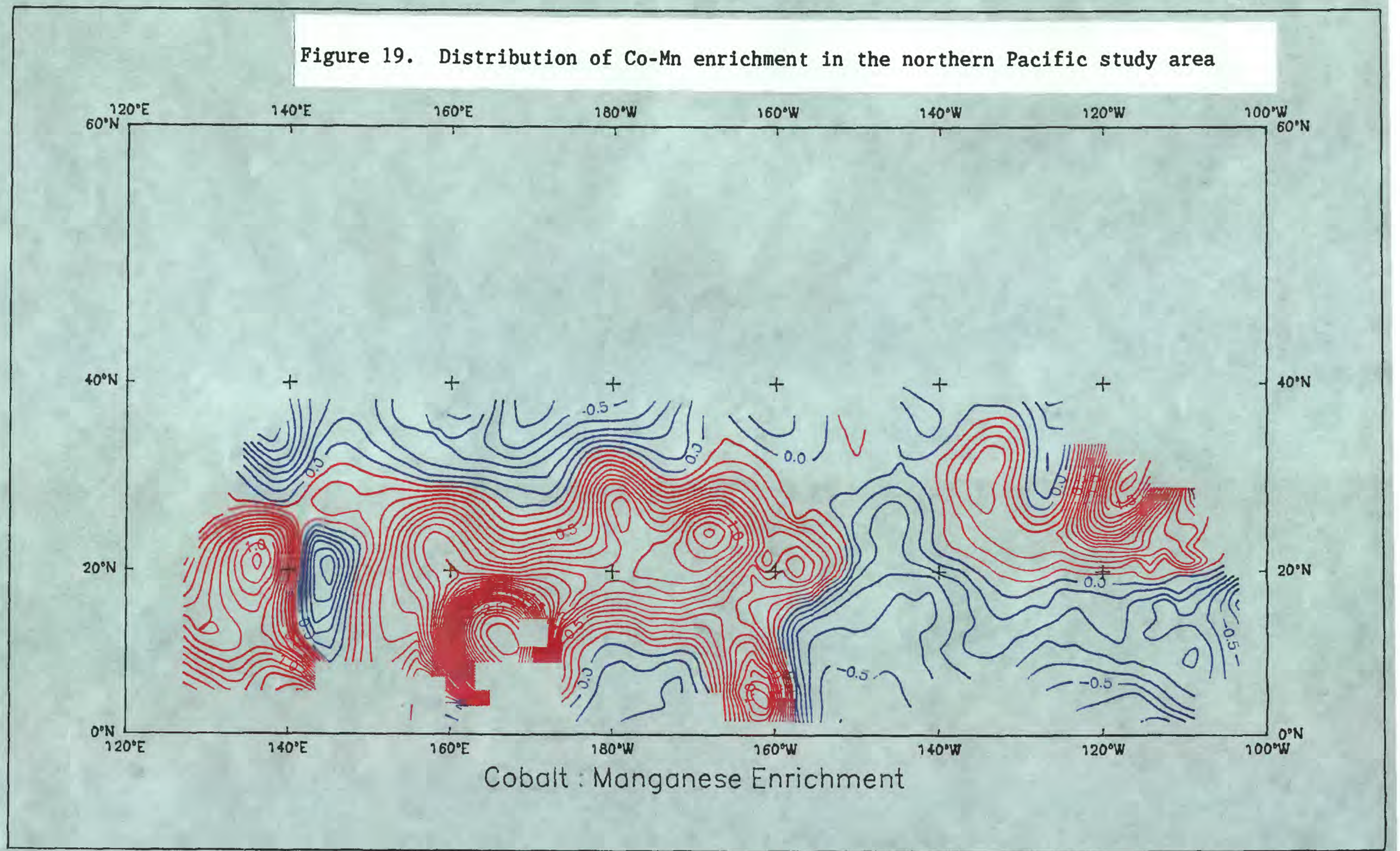

Figure 20. Distribution of Ni-Mn enrichment in the northern Pacific study area

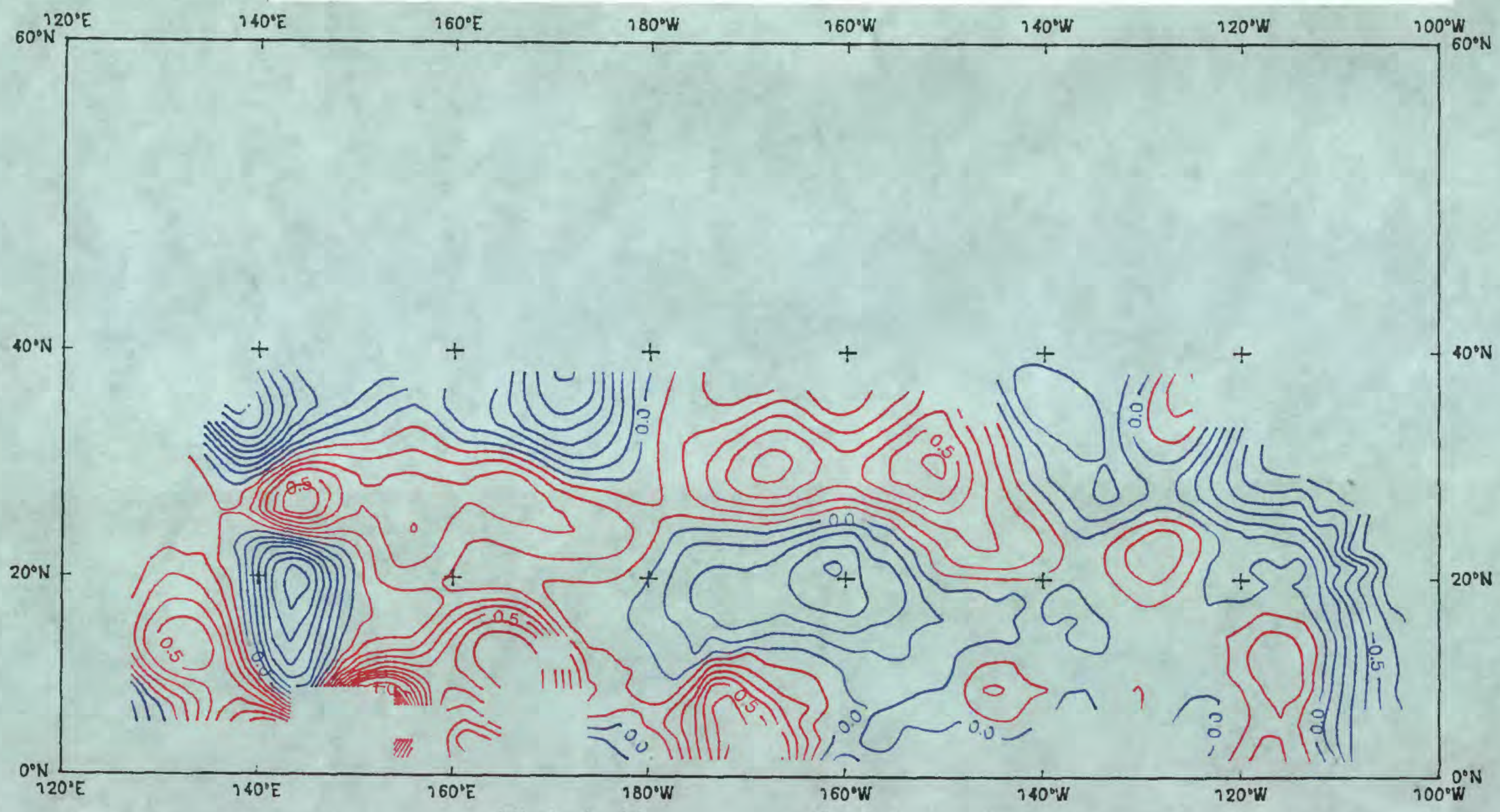

Figure 21. Distribution of Ni-Co enrichment in the northern Pacific study area

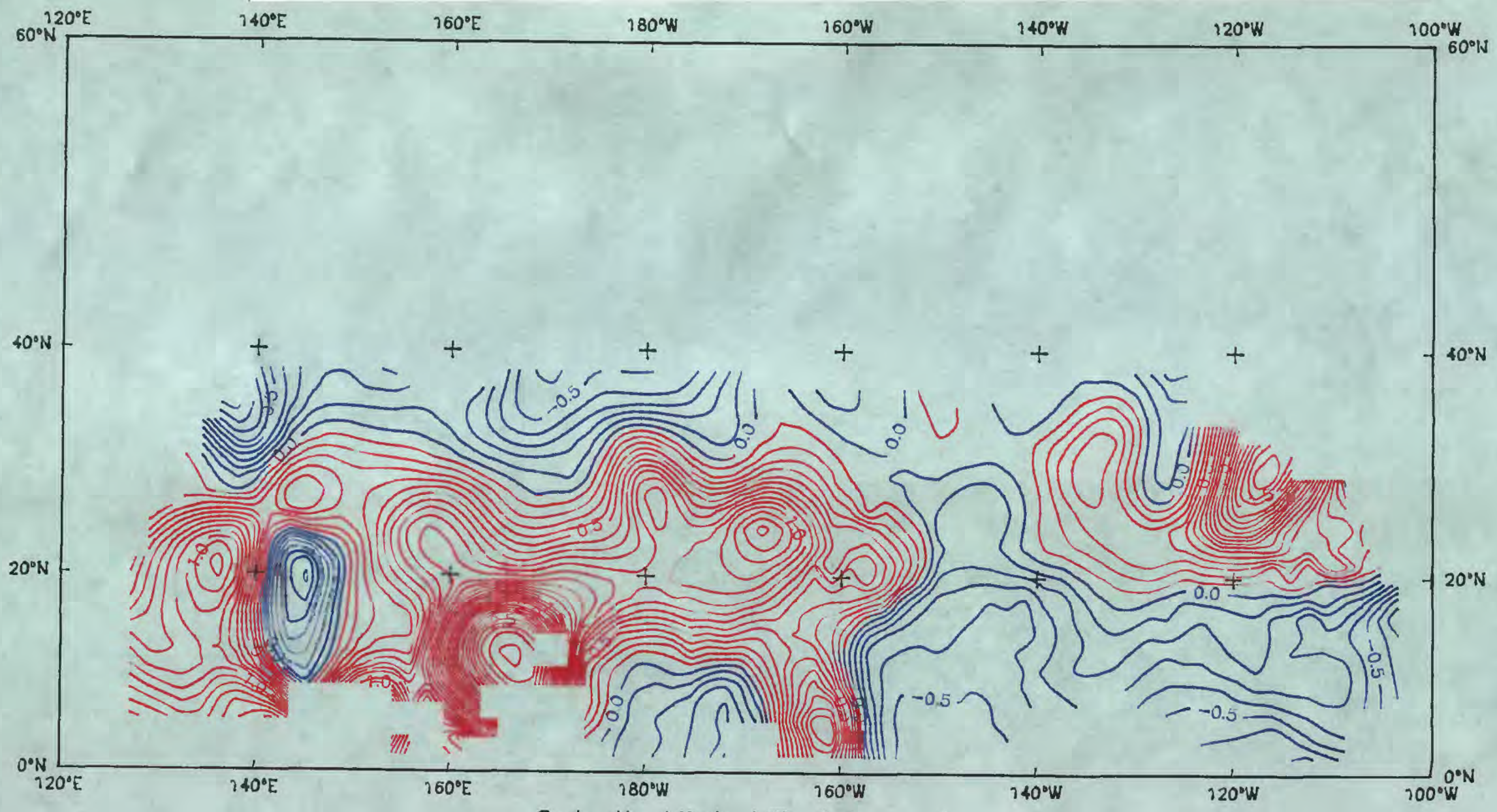

Figure 22. Distribution of Co-Ni-Mn enrichment in the northern Pacific study area